CHAPTER 2

Electron transfer in water and other polar environments, how it happens

David Chandler

Department of Chemistry, University of California, Berkeley, CA 94720

from: Classical and Quantum Dynamics in Condensed Phase Simulations, edited by B. J. Berne, G. Ciccotti and D. F. Coker (World Scientific, Singapore, 1998), pgs. 25-49.

Contents

1. – Marcus' scenario

Electron transfers – oxidation-reduction reactions – are among the most significant and universal of processes in chemistry and biology. In the realm of inorganic electrochemistry, the ferrous-ferric exchange in water,

$$\mathrm{Fe}^{2+}(\mathrm{aq}) + \mathrm{Fe}^{3+}(\mathrm{aq}) \rightleftharpoons \mathrm{Fe}^{3+}(\mathrm{aq}) + \mathrm{Fe}^{2+}(\mathrm{aq}), \tag{1}$$

is the simplest example. In the realm of biophysical chemistry, the photoinduced primary charge separation occurring in a photosynthetic reaction center is among the most complex examples. In the former case, at 1 M salt concentration, the process occurs once every 0.1 s. It is clearly a rare event. In the latter case, however, the process occurs rapidly, within 1 to 10 ps following photoexcitation. In both cases, the theoretical understanding of these processes is guided by phenomenology R. A. Marcus developed nearly a half century ago. For this development, Marcus was awarded the 1992 Nobel Prize in Chemistry.

Figure 1 illustrates schematically the general pathway to electron transfer, as it is envisaged in Marcus' theory. There are two localized electronic states pictured. These are the two redox states. In one, a transferable electron is located at site A; in the other, the transferable charge is located on site B. If the state with the electron at site A is the initial state, species A^- is called the "donor", and species B is called the "acceptor". In the ferrous-ferric exchange, A^- coincides with the ferrous ion, Fe^{2+}, and B coincides with the ferric ion, Fe^{3+}.

Most often, electron transfer occurs in a polar environment. In the aqueous ferrous-ferric exchange, this environment is created by water surrounding the iron ions. The asymmetric $A^- - B$ charge distribution is solvated by a polarized solvent. The precise nature of the solvation is not universal. For example, in the ferrous-ferric case, each of the iron ions is tightly coordinated to six water molecules, forming long lived octahedral complexes, as illustrated in Fig.2. The complexed waters are called "ligands". In the parlance of electron transfer theory, the ligands comprise the "inner shell" of solvent, and all other water molecules comprise the "outer shell". The charge distribution of the redox pair will polarize both inner and outer shells. In the former case, the polarization is associated with a distortion of the octahedral ligand-ion bonding. In the latter, it is associated with a dipolar field of the surrounding solvent that might be approximately described by dielectric continuum theory.

In either case, a polar environment organizes around an asymmetrical charge distribution in such a way as to give favorable solvation energy. The loss of asymmetry in the charge distribution will therefore be associated with a loss of that favorable energy. In other words, passing from a state in which electronic charge is localized on one redox center to a state where the charge is distributed over two redox centers will be associated with an increase in energy. The charge distributed or resonating state is the transition state for electron transfer, and the increase in energy to reach that state is the activation energy for electron transfer. Once attained through some random thermal fluctuation of

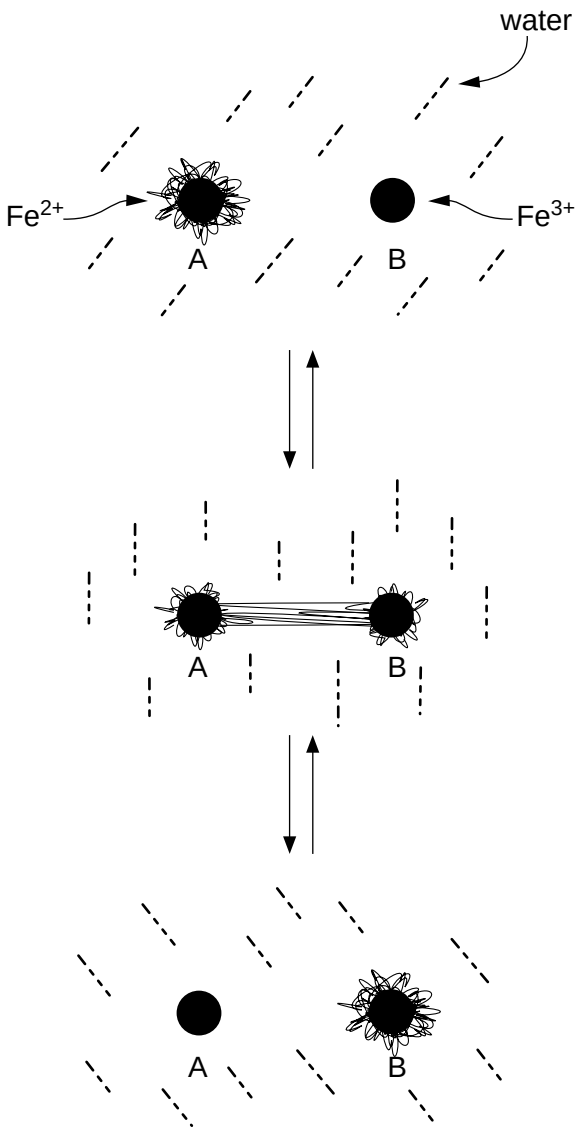

Fig. 1. – The Marcus scenario of electron transfer. An electron initially resides on redox site A (e.g., corresponding to the ferrous ion, Fe^{2+}). In this electronic state, A^-B, as depicted in the upper part of the figure, a typical equilibrium configuration of the environment (e.g., surrounding water) is polarized, giving a favorable (i.e., negative) interaction energy between the redox pair and the environment. With this environmental configuration, the energy of the A^-B state is far below that of the AB^- state. A not typical environmental fluctuation, however, can produce a configuration where A^-B and AB^- are degenerate. Here, since the favorable solvation energy is lost, the energy will be generally higher than that of the stable initial state. Since the two redox states are degenerate, the electron will resonate between the two redox centers, as depicted in the central portion of the figure. It is the transition state for electron transfer since once attained, the system can move quickly (and downhill in energy) to the other redox state, AB^-, depicted in the bottom of the figure.

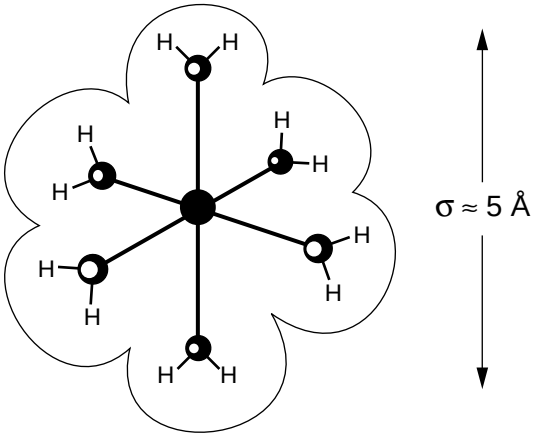

Fig. 2. – The octahedral structure of hexa aqua ferrous and ferric complexes. The oxygen iron bonds are 2.0Å and 2.1Å for the Fe^{2+} and Fe^{3+} ions, respectively, thus forming space filling octahedral clusters that are roughly 5Å in diameter.

the environment, the system — the redox pair plus environment — can move downhill in energy or free energy either by falling back to where it started, or by falling towards the other charge localized state, $A - B^-$. In the latter case, electron transfer occurs.

In this scenario, depicted in Fig.1, electron transfer occurs due to environmental fluctuations. The stable redox states correspond to solvated asymmetrical charge distributions. If one imagined an instantaneous electron transfer when one of the redox states was solvated, there would be a huge cost in energy. The transfer would therefore not occur without an external stimulus, such as a photoexcitation. For it to happen in the dark, the energy required for electron transfer must come from the bath – the surrounding solvent. In other words, the transition state is accessed through a fluctuation of the molecular environment. This temporal reorganization creates a situation where the two redox states are degenerate, neither is preferred energetically. At such a stage, with degenerate redox states, the electron will resonate between both sites. The electron will localize again only after the environment moves towards one of the two solvated configurations. Schematically, therefore, the reaction coordinate for electron transfer is the solvent polarization or local electric field. The transition state corresponds to that field where the two redox states are degenerate.

2. – From the perspective of the electron

To build a quantitative theory from this picture, a Hamiltonian is needed. And to build the Hamiltonian, it is useful to first consider the system from the context of the transferring electron.

Imagine the potential energy felt by an electron in the field of two degenerate redox sites [e.g., two $Fe^{3+}(H_2O)_6$ complexes] a distance $R = z_B - z_A$ apart, as depicted in Fig.3. For this potential field, $V(z)$, it is natural to construct electronic eigen states from linear combinations of states centered on one or the other sites, $|A\rangle$ and $|B\rangle$. If E_0 is the ground state energy when the electron is localized at one of these centers, the lowest

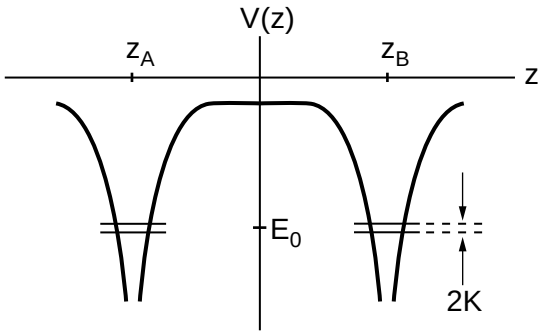

Fig. 3. – Potential energy for an electron moving in the field of two degenerate redox sites. The two lowest energy levels are $E_0 \pm K$, where K is the electron tunneling amplitude given by Eq.(2).

pair of energy levels are then $E_0 \pm K$. Here,

$$-K = \langle A|H_0|B\rangle \quad , \tag{2}$$

where H_0 denotes the Hamiltonian of the electron in the field of the two degenerate redox sites. Since the tails of wave functions are exponential, overlap integrals decay exponentially. Indeed, for a variety of electron transfer systems, detailed calculations demonstrate that

$$K \approx K_\sigma e^{-(R-\sigma)/\xi} \quad , \tag{3}$$

where σ is a typical distance of closest approach between two redox pairs, e.g., $\sigma \sim 5$Å, $K_\sigma \sim 10^2 \mathrm{cm}^{-1}$ (roughly the thermal energy, $k_\mathrm{B}T$, at room temperature), and $\xi \sim 1$Å. The gap between the ground and first excited state is therefore relatively small.

To the extent that only the two lowest energy states are relevant (the other electronic states are typically much higher in energy), E_0 can be taken as the zero of energy, and the electron coupled to the two redox sites is described by the two state Hamiltonian,

$$H_0 = \begin{bmatrix} 0 & -K \\ -K & 0 \end{bmatrix} \quad . \tag{4}$$

The introduction of solvent and ligand structure will alter this Hamiltonian. In particular, the electric field associated with temporal reorganization or distortion of the solvent and ligand structures will generally alter $V(z)$ from the symmetrical form drawn in Fig.3 to the asymmetrical form drawn in Fig.4. Solvation produces a large energy gap, ΔE, between the ground and first excited state. The excited state coincides with moving charge from the solvent stabilized site to the solvent destabilized site. The typical size of the gap can be estimated by juxtaposing the Born solvation energies of a static dipole (corresponding to the electronic charge localized on, say, redox site A) with that of a resonating dipole (corresponding to the charge distributed on the two redox sites). These two cases are illustrated in Fig. 5. In the former case, the solvation energy is due to the reaction field of the statically polarized solvent. It is given by

$$E^{(A)}_{\mathrm{solvation}} \approx -(e^2/a)(1 - 1/\epsilon), \tag{5}$$

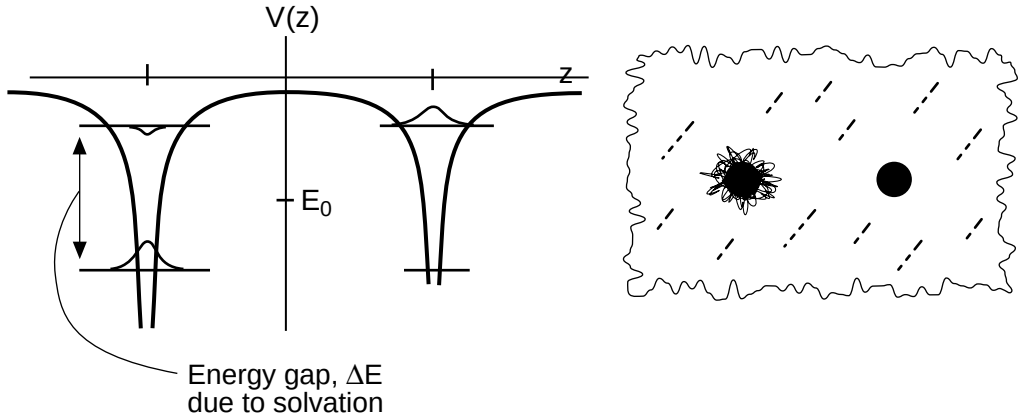

Fig. 4. – Potential energy (left) for an electron moving in the field of two redox centers plus a polarized solvent (depicted at right).

where a is a typical microscopic length, of the order of σ, and ϵ is the static dielectric constant of the solvent. In the latter case, the oscillations of the electronic dipole are too fast to couple to the much slower nuclear motions of the solvent (e.g., reorientations of the surrounding water). In this case, therefore, only the electronic polarizability can lead to solvation of the redox pair. Thus, here, the solvation energy is given by

$$E^{(\mathrm{TS})}_{\mathrm{solvation}} \approx -(e^2/a)(1 - 1/\epsilon_\infty), \tag{6}$$

where ϵ_∞ is the optical dielectric constant of the solvent.

For water (where $\epsilon \approx 80$) and other highly polar solvents, $1 - 1/\epsilon \approx 1$. On the other hand, typically, $\epsilon_\infty \approx 2$. Thus,

$$\Delta E \sim (e^2/a)(1/\epsilon_\infty - 1/\epsilon) \approx e^2/a\epsilon_\infty \sim 1\,\mathrm{eV}. \tag{7}$$

3. – From the perspective of the solvent nuclei

Assuming only two electronic states are pertinent, the full Hamiltonian of the system can be generally written as

$$\begin{aligned} H &= \begin{bmatrix} 0 & -K \\ -K & -\Delta\epsilon \end{bmatrix} - \mathcal{E}\begin{bmatrix} -1 & 0 \\ 0 & 1 \end{bmatrix} + H_{\mathrm{b}}(x_1, x_2, \ldots, x_N)\begin{bmatrix} 1 & 0 \\ 0 & 1 \end{bmatrix} \\ &= \begin{bmatrix} H_A & -K \\ -K & H_B \end{bmatrix} \quad . \end{aligned} \tag{8}$$

Here, the first matrix to the right of the first equality represents the Hamiltonian of the redox pair when it is uncoupled to the environment. It corresponds to that written in Eq.(4), but generalized to account for the fact that the redox pair might be asymmetric.

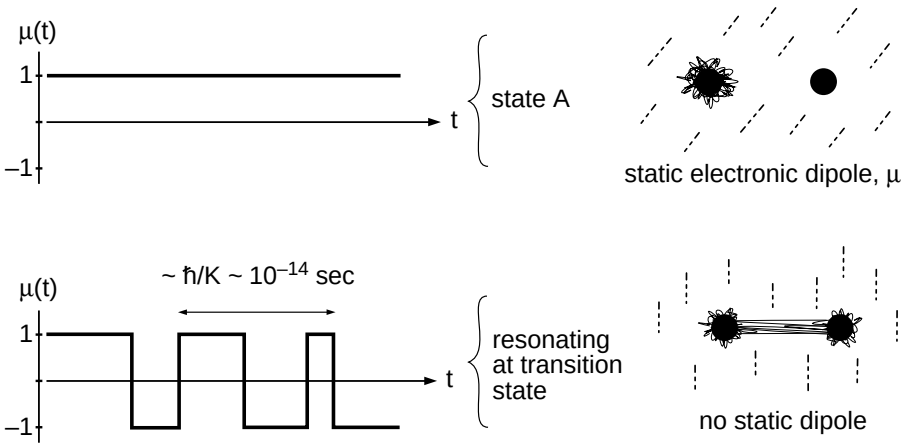

Fig. 5. – Solvation of a static unit dipole and solvation of a resonating dipole. In the static case, the path of the dipole, $\mu(t)$, is a constant – 1 for the electron localized on site A. In the resonating case, the path of the dipole is oscillatory, between 1 and -1, with period given by $\hbar/K$.

For the symmetric $Fe^{2+} - Fe^{3+}$ exchange, $\Delta\epsilon = 0$. The second term can be viewed schematically as the coupling between a unit dipole of the redox pair and the local electric field, $\mathcal{E}$. More precisely, and generally, $-2\mathcal{E}$ is the environment's contribution to the energy gap between the two charge localized redox states. The total energy gap, ΔE, is given by

$$\Delta E = H_B - H_A = -2\mathcal{E} - \Delta\epsilon \quad , \tag{9}$$

where H_B is the Hamiltonian of the entire system, redox pair plus environment, when the transferring electron is localized at site B (i.e., redox pair is confined to state AB^-), and H_A is similarly defined for the case where the electron is localized on site A (i.e., the redox pair is confined to state A^-B).

There are many dynamical variables that contribute to $\mathcal{E}$. For example, major contributions come from interactions between solvent dipoles and the charges on the redox pair, and each of these interactions is determined by the orientational and translational coordinates of the solvent molecules. Schematically, we denote these coordinates as the set of variables $x_1, x_2, \ldots, x_N$. We denote the Hamiltonian that controls them in the absence of the redox pair by $H_{\rm b}(x_1, x_2, \ldots, x_N)$. The subscript "b" stands for "bath".

For many situations, we expect that $\mathcal{E}$ obeys Gaussian statistics. The reason is two fold, as we can discuss specifically for the aqueous ferrous-ferric exchange. First, the structures of the ligands are nearly rigid. The fluctuations in their structures can therefore be viewed in terms of small amplitude oscillations of atomic coordinates. Because their amplitudes are small, these oscillations are well described by a harmonic oscillator approximation. The Boltzmann statistics of harmonic oscillator variables is Gaussian.

Second, the interactions between the redox pair and the outer solvation shell is essentially a sum of many long ranged dipole-charge interactions. Yet the correlation length of liquid water is small, of the order of the diameter of a water molecule, about 3Å. Thus, the outer shell contribution to $\mathcal{E}$ is a superposition of many statistically independent

entities. The central limit theorem suggests that such a variable is Gaussian.

The probability distribution for $\mathcal{E}$ is proportional to the Boltzmann factor for the reversible work or free energy of that variable. Let

$$P_{\rm b}(\mathcal{E}) \propto \exp[-\beta F_{\rm b}(\mathcal{E})] \tag{10}$$

denote that function in the absence of the redox ions (i.e., for the pure bath). With no redox pair, the average polarization is zero. That is, $\langle \mathcal{E} \rangle_{\rm b} = 0$. Thus, assuming the statistics of $\mathcal{E}$ is Gaussian, we have

$$F_{\rm b}(\mathcal{E}) = \frac{1}{2\alpha}\mathcal{E}^2, \tag{11}$$

where α is related to the mean square amplitude of energy gap fluctuations by the principle of equipartition. In particular,

$$\langle \mathcal{E}^2 \rangle_{\rm b} = \alpha/\beta = k_{\rm B}T\,\alpha\,. \tag{12}$$

In most configurations of the environment, the interstate coupling element, K, is typically small compared to the energy gap. Were this coupling zero, electron transfer would not occur, and the localized redox states would be eigen states of the Hamiltonian.

When the electron is localized on site A, the reversible work for changing the energy gap is given by

$$F_A(\mathcal{E}) = \frac{1}{2\alpha}\mathcal{E}^2 + \mathcal{E}\,. \tag{13}$$

When the electron is localized on site B, however the reversible work is given by

$$F_B(\mathcal{E}) = \frac{1}{2\alpha}\mathcal{E}^2 - \mathcal{E} - \Delta\epsilon\,. \tag{14}$$

Figure 6 illustrates these functions for the symmetric aqueous ferrous-ferric exchange example, where $\Delta\epsilon = 0$. The interstate coupling is relevant in the region where the two free energy functions are close in energy. If nuclei move very slowly, this region can be described adiabatically. This is done by treating $\mathcal{E}$ as a constant and determining the states that diagonalize the resulting 2×2 Hamiltonian (8). The result of this treatment is illustrated in Fig.6. At the point where the two localized states are degenerate, this procedure splits this degeneracy, giving two eigen energies, one at $-K$ and the other at $+K$. When the coupling K is neglected, the two eigen states are called "diabatic" states. Their corresponding free energy functions are the intersecting parabolas (13) and (14). When nuclear dynamics is neglected, the two eigen states are called "adiabatic" states. Except where the diabatic states are close in energy, the ground adiabatic state is the diabatic state of lowest energy, and the excited adiabatic state is the diabatic state of highest energy. Where the diabatic states are close in energy, however, the interstate coupling K cannot be neglected. The two adiabatic states are mixtures of the diabatic states, and their energies are non intersecting functions of $\mathcal{E}$.

To the extent that the statistics of $\mathcal{E}$ is Gaussian, the bath variables, $x_1, \ldots, x_2$, can be viewed as a collection of harmonic oscillator coordinates, and $\mathcal{E}$ is a linear combination of these oscillator coordinates. In this circumstance, the Hamiltonian (8) is equivalent to that for a bosonic bath coupled to a quantized 1/2 spin. Due to this equivalence, the model Hamiltonian has acquired the name "spin boson". Much recent theoretical work

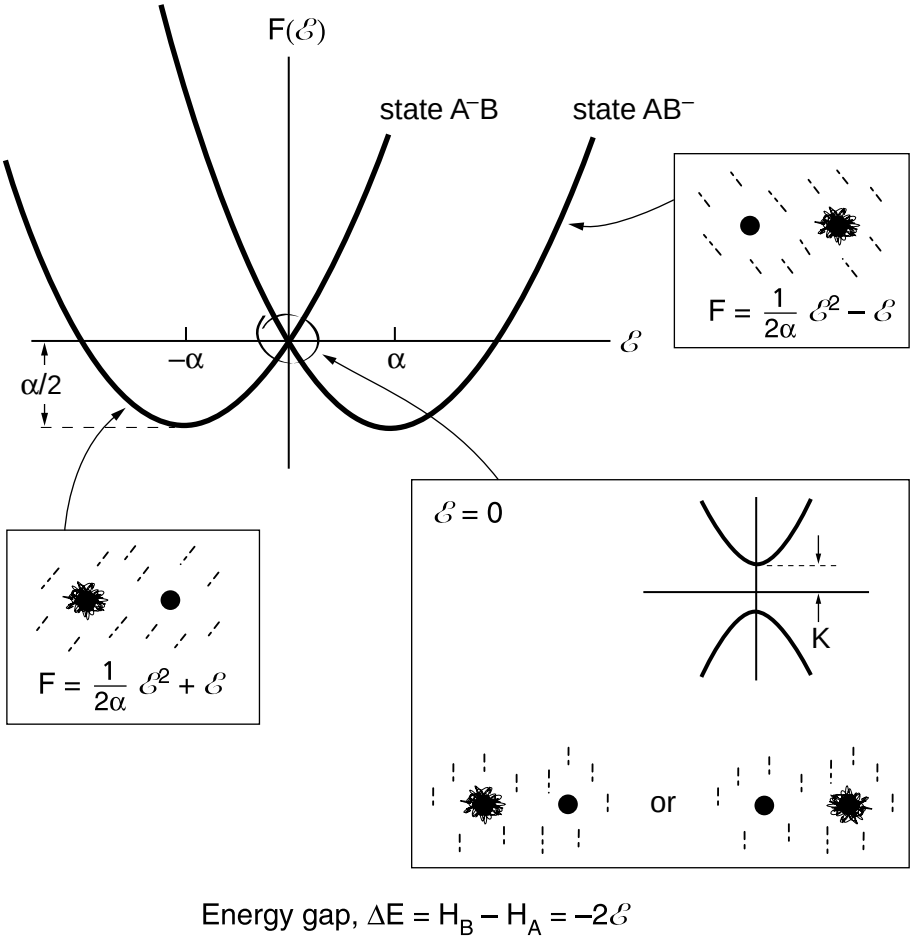

Fig. 6. – Free energy functions for symmetric charge transfer states. The lower left and upper right insets depict the respective equilibrium structures of their respective stable states, and give the algebraic form of their free energies as functions of the energy gap variable, $\mathcal{E} = -\Delta E/2$. The lower right inset focuses on these functions near $\mathcal{E} = 0$, illustrating the splitting of adiabatic states due to the resonance between the two degenerate localized redox states.

done on this model is concerned with the nature of quantum coherence. Coherence is associated with persistent resonance, slowly dephased by fluctuations in the environment. The interstate coupling K must be substantial in this regime. In contrast, our use of the spin boson model is confined to the incoherent regime where K is small. In particular, when electron transfer occurs, it does so as a rare event with a well defined rate constant, with the state of a resonating electron existing only briefly, at the transition state. We will soon address the task of computing the rate constant for the model. We first pause, however, to note that computer simulation studies have tested the accuracy of the Gaussian approximation underlying the spin boson model.

4. – Test of the Gaussian approximation

The distribution of energy gaps in the A^-B diabatic state is

$$P_A(\mathcal{E}) = \left\langle \delta\Big[\mathcal{E} + \frac{1}{2}(H_B - H_A)\Big]\right\rangle_A \quad , \tag{15}$$

where $\langle\cdots\rangle_A$ denotes the equilibrium average over solvent configurations when the transferable charge is localized on site A. This distribution can be determined through computer simulation, employing a form of umbrella sampling. For the aqueous ferrous-ferric system, for example, H_A corresponds to the a classical Hamiltonian with the redox pair confined to the $Fe^{2+} - Fe^{3+}$ state, and H_B is that for the $Fe^{3+} - Fe^{2+}$ state. These Hamiltonians can be estimated in terms of a water-water pair potential, a ferrous ion-water potential, and a ferric ion-water potential. Then, with the two iron ions fixed at a given interionic separation, immersed in a container of several hundred water molecules and periodically replicated, a series of classical trajectories can be performed with various choices of the intermediate Hamiltonian,

$$H_\lambda = H_A + \lambda\,(H_B - H_A) \quad . \tag{16}$$

By varying the value of λ between 0 and 1, the system can be moved reversibly from one redox state to the other (as if the electronic charge could be moved in partial stpdf from one center to the other). On the way, at each intermediate value of λ between 0 and 1, a histogram of energy gap values can be tabulated. These histograms can then be weighted and overlapped to form the continuous distribution according to the usual Boltzmann distribution law

$$\begin{aligned} P_A(\mathcal{E}) &\propto \left\langle \delta\Big(\mathcal{E} + \frac{1}{2}\Delta E\Big) e^{\beta\lambda\Delta E}\right\rangle_\lambda \\ &= \left\langle \delta\Big(\mathcal{E} + \frac{1}{2}\Delta E\Big)\right\rangle e^{-2\beta\lambda\mathcal{E}} \quad , \end{aligned} \tag{17}$$

where

$$\Delta E = H_B - H_A = -2\mathcal{E} \quad , \tag{18}$$

coinciding with Eq.(9) for the symmetric exchange (i.e., $\Delta\epsilon = 0$).

Figure 7 shows the results of such a calculation performed for the aqueous ferrous-ferric exchange. To a remarkable extent, over an energy range of several eV, the diabatic free energies are parabolic. Thus, the energy gap distributions are essentially Gaussian. For example, for the symmetric exchange, the free energies (13) and (14) intersect where $\mathcal{E} = 0$, and at this point, the value of the free energies should be related to their values at the average and most probable energy gap, $\langle\Delta E\rangle_A$, according to

$$F(0) - F(\langle\mathcal{E}\rangle_A) = \frac{1}{4}\langle\Delta E\rangle_A \,. \tag{19}$$

Figure 7 shows that this relationship holds quantitatively.

The same atomistic model used for computing the distribution of energy gaps has been used to examine non-equilibrium relaxation. This study further validates the use of the spin boson type model as a realistic caricature of electron transfer systems. Specifically, consider the simulation of photoexcitation depicted in Fig.8. Several hundred statistically independent phase space points are taken from a long equilibrated run of

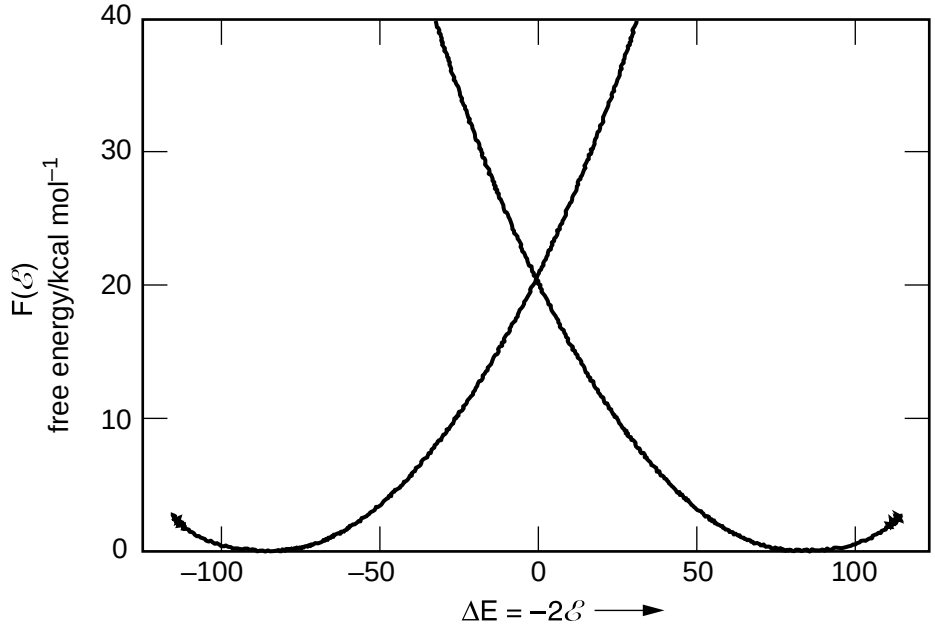

Fig. 7. – Diabatic state free energy functions for a computer simulation model of the aquious ferrous-ferric exchange, computed by umbrella sampling at room temperature, with the $Fe^{2+} - Fe^{3+}$ separation fixed at 5.5Å. Adapted from R. A. Kuharski *et al., J.Chem.Phys.***89**, 3248 (1988).

aqueous $Fe^{2+} - Fe^{3+}$. For each, the redox pair is suddenly switched to $Fe^{3+} - Fe^{2+}$, as if the system adsorbed the excitation of a photon. The altered electrostatic field caused by the new charge state of the solute pair places the solvent in a highly energetic configuration. In the dynamics that follows, the solvent reorganizes to lower its energy and to solvate the new charge state. The resulting change in energy gap, averaged over all the trajectories run in this way, is graphed in the main panel of Fig.8. Plotted with it is the energy gap autocorrelation function, scaled and shifted so as to have the same initial and final values as the averaged non-equilibrium energy gap. The autocorrelation function is computed in the usual way from an equilibrium time average:

$$\langle \mathcal{E}(0)\mathcal{E}(t)\rangle_A = \frac{1}{\mathcal{N}} \sum_{i=0}^{\mathcal{N}} \mathcal{E}(t_i)\mathcal{E}(t_i + t)\,. \tag{20}$$

Here, the t_i's, with $0 \le i \le \mathcal{N}$, are points in time on a long trajectory equilibrated in the electron localized on site A (corresponding, say, to the ferrous-ferric state).

If the statistics of $\mathcal{E}$ is Gaussian, the non-equilibrium relaxation should agree closely with the scaled and shifted autocorrelation function. This fact can be understood in two ways. First, if the statistics is Gaussian, the dynamics of the environment can be thought of as that of a bath of harmonic oscillators. Dynamical frequencies for harmonic oscillators are independent of energy or coordinate amplitude. Thus, the relative motions of $\mathcal{E}$ during relaxation from a highly excited state should scale as those associated with spontaneous fluctuations about the average equilibrium state. Second, if the statistics is Gaussian and thus equivalent to that of a bath of harmonic oscillators, the response

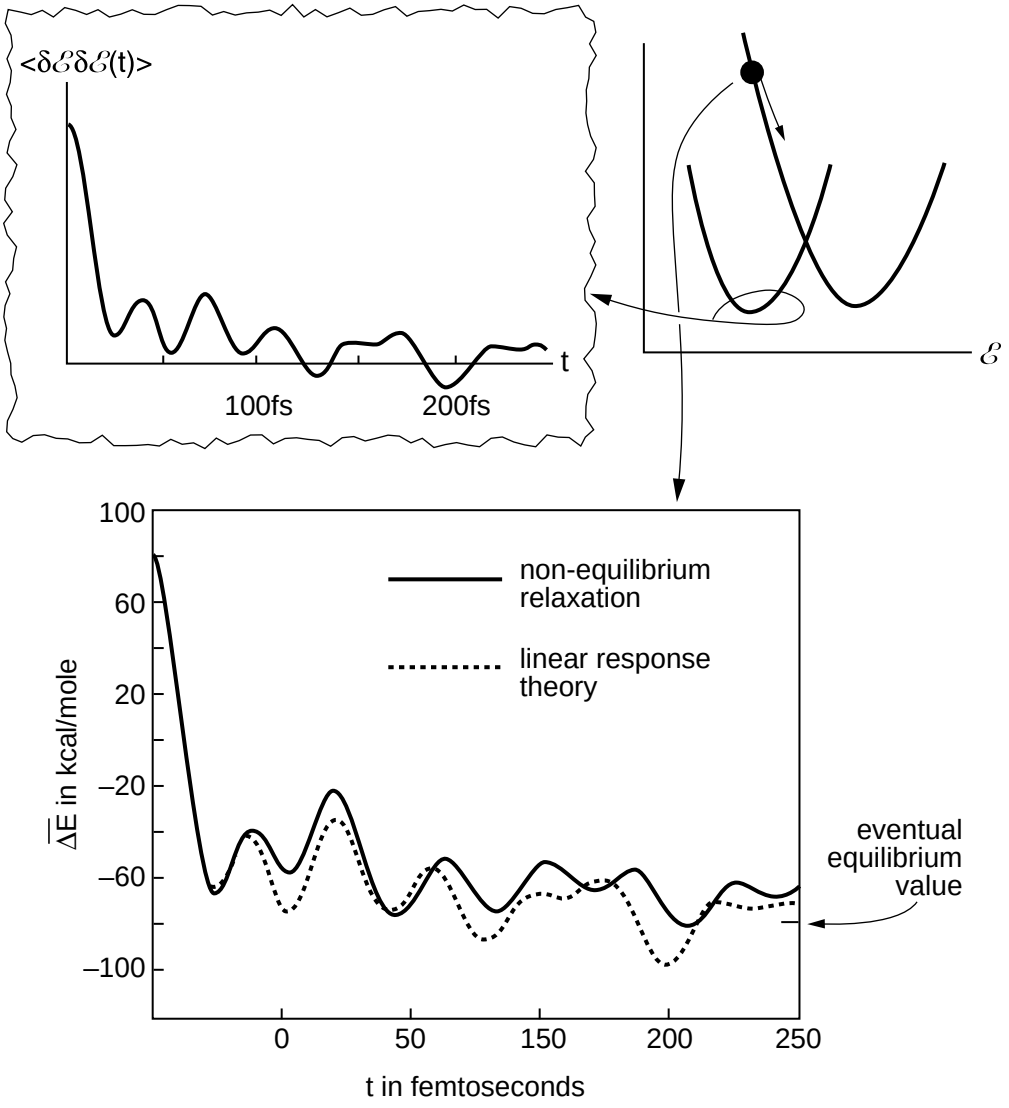

Fig. 8. – Computer simulation of relaxation after photoexcitation compared with autocorrelation of spontaneous fluctuations in the stable state. The upper right insert depicts the diabatic free energy surfaces pertaining to this charge transfer system, the aqueous ferrous-ferric redox pair, and an initial non equilibrium configuration immediately following excitation. The subsequent interstate energy gap relaxation, averaged over an ensemble of such initial conditions, is graphed as the solid line in the central panel. The upper left inset shows the energy gap fluctuation correlation function for one of the stable states, computed from a time displaced average over an equilibrium trajectory. Scaled and shifted, according to Eq.(21), this correlation function is plotted as the dashed line in the central panel to interpret the non equilbrium relaxation. Figure adapted from J. S. Bader and D. Chandler, *Chem.Phys.Lett.***157,**501(1989).

of $\mathcal{E}$ is linear. This assertion follows from the fact that restoring forces for harmonic oscillators are linear.

Since we expect the response to be linear, we expect that the fluctuation-dissipation theorem can be applied, giving

$$\frac{\overline{\Delta E}(t)}{\overline{\Delta E}(0)} = \frac{C(t)}{C(0)} \tag{21}$$

where the over bar on the left-hand-side indicates the non-equilibrium average (i.e., the average over the trajectories with initially prepared non-equilibrium configurations), and the function $C(t)$ denotes the auto correlation function, $\langle \delta\mathcal{E}(0)\delta\mathcal{E}(t)\rangle_A$, where $\delta\mathcal{E}(t)$ denotes the instantaneous fluctuation, $\mathcal{E}(t) - \langle\mathcal{E}\rangle_A$. Equation (21) states that to the extent Gaussian statistics is valid, the scaled and shifted correlation function should equal the non-equilibrium relaxation function. Figure 8 shows that Eq.(21) holds to a remarkable extent.

The relaxation depicted in Fig.8 neglects the possibility of back electron transfer when the system passes through the curve crossing region near $\mathcal{E} = 0$. This neglect is a good approximation to reality when the passage is very rapid. In particular, the probability of a transition between degenerate diabatic states is related to the interstate coupling by

$$p = 2\pi K^2 \Big/ \hbar \, \langle|\dot{\mathcal{E}}|\rangle^* \big|\partial F_A^*/\partial\mathcal{E} - \partial F_B^*/\partial\mathcal{E}\big| \tag{22}$$

where $\langle|\dot{\mathcal{E}}|\rangle^*$ is the average size of the rate of change of $\mathcal{E}$ at the point of degeneracy, and $-\partial F_{\rm A}^*/\partial\mathcal{E}$ is the average force on $\mathcal{E}$ at the point of degeneracy with the electron localized on site A. Equation (22) is the Landau-Zener transition rate formula. We leave its justification for later. We cite it here to show that this probability decreases with increasing velocity.

Figure 8 shows that the traversal is indeed rapid for the aqueous ferrous-ferric system. In roughly 10 to 20 fs, 3 eV of energy is dissipated into the solvent. One may combine this fact with the value for the curvature of the diabatic free energy functions to show that p is negligible, thus justifying the neglect of back electron transfer. Were passage through the transition state relatively slow, p would not be small. In that situation, corresponding to what is called "adiabatic electron transfer", nuclear dynamics is controlled by the Hellmann-Feynman forces — the forces determined by the electronic adiabatic ground state. This situation is not physically pertinent to aqueous electron transfer. Rather, since p is very small, aqueous electron transfer is highly non adiabatic. The rapid relaxation viewed in Fig.8 is due primarily to rapid orientational changes in water structure. These changes are librational motions. Since these motions occur on such a rapid time scale, some important aspects of water dynamics are intrinsically quantum mechanical. In particular, the librational frequency 0.05 fs^{-1} is larger than $k_{\rm B}T/h$. The relevance of this fact to thermal electron transfer kinetics will be discussed soon. First, however, a formula relating the electron transfer rate constant to solvent dynamics is required.

5. – Electron transfer rate constant

In the highly non adiabatic regime, the diabatic redox states are nearly stationary states. We can focus on these states, and use perturbation theory to describe how they

change in time. Let $|A\rangle$ and $|B\rangle$ denote the state vectors for these diabatic states, where the transferring electron is localized either on site A or site B, respectively. Then

$$h = |A\rangle\langle A| \qquad \text{or} \qquad h = \begin{bmatrix} 1 & 0 \\ 0 & 0 \end{bmatrix} \tag{23}$$

is the occupation or population operator of the A^-B state.

Following the logic of Lecture 1, the relevant reactive flux for this population is

$$k(t) = -\frac{d}{dt}\,\frac{\langle h\,\delta h(t)\rangle}{\langle h\,\delta h\rangle} \sim k_{\rm ET}\; e^{-k_{\rm ET}\,t} \quad , \tag{24}$$

where $k_{\rm ET}$ is the sum of forward and back electron transfer rate constants. The asymptotic equality holds for times larger than a transient relaxation plateau time. Due to the uncertainty principle, at thermal conditions, this time must at least be larger than $\beta\hbar$. For times smaller than transient times, quantum mechanical versions of Eq.(24) will include averages over an imaginary time $-i\tau$, where $0 < \tau < \beta\hbar$ — the so-called "Kubo transformations". Such averages cannot be neglected when considering short time behavior of the reactive flux. For times beyond transient times, however, the correlation function to be differentiated to give $k(t)$ can be expressed formally as

$$\langle h\,\delta h(t)\rangle = {\rm Tr}\; e^{-\beta H} h\; e^{iHt/\hbar}\; \delta h\; e^{-iHt/\hbar} \Big/ {\rm Tr}\; e^{-\beta H}, \tag{25}$$

where "Tr" denotes the trace over states of the redox pair, $|A\rangle$ and $|B\rangle$, and the environment. For the spin boson caricature, the environmental states are vibrational states of the bath of oscillators.

The interstate coupling K is the small parameter in the Hamiltonian (8). By expanding in powers of this parameter, one finds for the forward rate constant

$$k_{A\to B} = \frac{K^2}{\hbar^2} \int_{-\infty}^{\infty} dt\; \langle e^{iH_A\,t/\hbar} e^{-iH_B\,t/\hbar}\rangle_A + O(K^4) \tag{26}$$

where

$$\langle \cdots \rangle_A = {\rm Tr}\; e^{-\beta H_A}[\cdots] \Big/ {\rm Tr}\; e^{-\beta H_A} \tag{27}$$

denotes the thermal average over states of the bath when the redox system is confined to state A. A similar expression is found for the back rate. To consistent orders of K, the forward and back rate constants obey detailed balance. Neglecting the terms higher order than K^2, Eq. (26) is Fermi's so-called "golden rule" formula for the rate constant.

In general, H_A and H_B do not commute. But if the environment is classical (i.e., if the frequencies of the spin boson oscillators are all small compared to $1/\beta\hbar$), the two phase factors in Eq.(26) can be combined into one factor. The integration over time can then be performed yielding a Dirac delta function,

$$\begin{aligned} [k_{A\to B}]_{\rm cl} &= \frac{2\pi K^2}{\hbar}\; \langle \delta(H_A - H_B)\rangle_A \\ &= \frac{2\pi K^2}{\hbar} \langle \delta(\Delta E)\rangle_A . \end{aligned} \tag{28}$$

The subscript "cl" emphasizes that this formula for the electron transfer rate constant is the classical approximation to the golden rule rate constant. The averaged delta function

is the probability density of observing a bath fluctuation with $\Delta E = 0$ when the system is in redox state $A^- B$. Thus,

$$[k_{\rm ET}]_{\rm cl} \sim K^2 e^{-\beta F^*}, \tag{29}$$

where

$$F^* = F_A(\mathcal{E}^*) - F_A(\langle \mathcal{E} \rangle_A). \tag{30}$$

Here, $\mathcal{E}^* = -\Delta\epsilon/2$. It is the value of $\mathcal{E}$ where the two redox states are degenerate. Assuming the statistics of $\mathcal{E}$ is Gaussian (i.e., the free energy functions are parabolic), $\langle \mathcal{E} \rangle_A$ is the value of $\mathcal{E}$ where $F_{\rm A}(\mathcal{E})$ is a minimum. Applying Eqs. (13) and (14), therefore, yields

$$F^* = \frac{1}{8\alpha}(\Delta\epsilon - 2\alpha)^2, \tag{31}$$

and Marcus' "energy gap law" for the electron transfer rate constant,

$$k_{\rm ET} \sim K^2 \exp[-(\beta/8\alpha)(\Delta\epsilon - 2\alpha)^2]. \tag{32}$$

The quantity F^* is the activation energy for the forward electron transfer.

6. – Reorganization energy and the normal and inverted regimes

In the usual terminology of electron transfer theory, the quantity 2α is called the "reorganization energy", and it is usually given the symbol λ. That is,

$$2\alpha = \lambda. \tag{33}$$

For polar fluids, a rough estimate of its size can be made with dielectric continuum theory. Following the arguments given in Sec. 2, such an estimate gives

$$\lambda \approx \frac{e^2}{a}\Big(\frac{1}{\epsilon_\infty} - \frac{1}{\epsilon}\Big). \tag{34}$$

Typical values are therefore in the range of 1 eV. For instance, the computer simulation results graphed in Fig.7 give a curvature corresponding to $\lambda \approx 3$ eV . Experimental measurements of λ for water give numbers in the range of 2 eV.

Part of the reorganization energy involves energy gap fluctuations associated with short ranged interactions. For example, in polar fluids, fluctuations in ligand structure contribute. The reorganization energy is not, therefore, entirely a universal property of the solvent. This source of system specificity, however, is relatively small. For nonpolar fluids, Eq.(34) would suggest that $\lambda = 0$ since in that case the net dielectric constant is essentially the optical dielectric constant. In reality, λ is relatively small for electron transfer in non polar fluids, but it is not at all zero. In liquid benzene, for example, reorganization energies are in the range of 0.2 to 0.6 eV.

One way of estimating the reorganization energy from experiment is to study the variation of electron transfer rate with thermodynamic driving force or exothermicity. In the Gaussian approximation, there is no entropy change for an electron transfer reaction. As such, $\Delta\epsilon$ is a measure of either the Gibbs free energy change or the exothermicity of the reaction. From Eq.(32), we see that the maximum electron transfer rate is attained

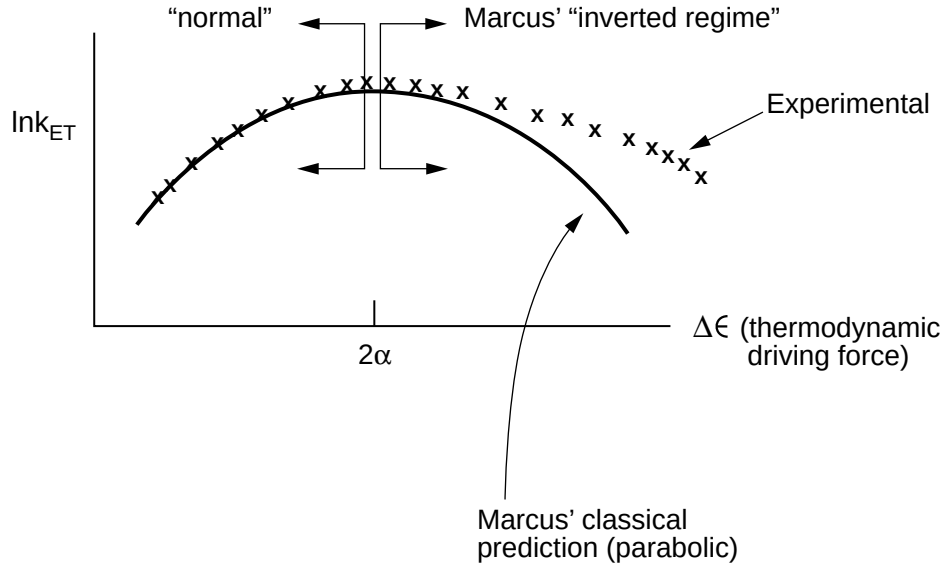

Fig. 9. – Variation of electron transfer rate with thermodynamic driving force. The inverted and normal regimes correspond to the thermodynamic driving force, $\Delta\epsilon$, being larger and smaller, respectively, than the reorganization energy, $\lambda = 2\alpha$. Experiments verify the prediction that $\ln k_{\rm ET}$ is a non monotonic function of driving force. In the inverted regime, however, experiments differ substantially from the classical prediction of an inverted parabolic functional form.

when $\Delta\epsilon = \lambda$. Finding that maximum as a function of exothermicity therefore determines the reorganization energy.

At this point of maximum rate, the electron transfer process is activationless. Here, the product free energy surface, $F_B(\mathcal{E})$, intersects the reactant surface, $F_A(\mathcal{E})$, at the point where the latter is a minimum. The transition state is at the point of the stable reactant state. For processes more exothermic, i.e., when $\Delta\epsilon > \lambda$, the electron transfer rate will decrease with increasing exothermicity. This regime is called Marcus' inverted regime. When $\Delta\epsilon < \lambda$, the opposite occurs — rates increase with increasing exothermicity. This regime is known as the normal regime.

The qualitative predictions of Marcus' energy gap law, Eq.(32), is illustrated in Fig. 9. The existence of the inverted region was considered a most striking and counter intuitive result. Its verification by John Miller and Gerhard Closs is often cited as the pivotal experiment leading to Marcus' Nobel Prize. While its existence is correctly predicted by the classical theory, the quantitative behavior of the rate as a function of $\Delta\epsilon$ is not correctly given by the classical theory. In particular, pathways involving nuclear tunneling become especially prevalent in the inverted region. These pathways augment those that are allowed classically. Thus, for a given value of $|\Delta\epsilon - \lambda|$, the rate is larger in the inverted region than in the normal region. This fact is illustrated in Fig. 9. To describe it quantitatively, we need to analyze Eq.(26) in the quantum mechanical realm.

7. – Quantum mechanical electron transfer rate constant

In general, the evaluation of the integral in Eq.(26) is non trivial. The integrand is a highly oscillatory function of time. Direct numerical evaluation is numerically unstable. Amelioration in such a circumstance is found through a stationary phase analysis. A stationary phase point lies on the imaginary time axis. For symmetric electron transfer, as in the case of the ferrous-ferric exchange, it is at the midpoint, $-i\beta\hbar/2$. In general, the stationary phase point must be found numerically. Once found, the exact evaluation of the integral can be done by displacing the line of integration off the real axis so as to pass through the stationary phase point. A useful analytical approximation expands the logarithm of the integrand to quadratic order about the stationary phase point, and performs the integration as if the integrand were Gaussian in time.

With computer simulation, this program can be carried out exactly by exploiting the isomorphic polymer representation of imaginary time quantum path integration. To the extent that the energy gap statistics is Gaussian, however, significant analytical reduction is possible. In particular, for a bath of oscillators, the stationary phase evaluation of Eq.(26) gives

$$k_{A\to B} \approx \frac{2\pi}{\hbar} K^2 \Big| \theta^3(t^*) \Big/ 2\pi\hbar\theta''(t^*) \Big|^{1/2}, \tag{35}$$

where

$$\theta(t) = \exp\Big\{ -\frac{1}{4\pi\hbar}\int_0^\infty d\omega\beta\hat{C}(\omega)\Big[\cosh(\beta\hbar\omega/2) - \cosh\Big(\frac{\beta\hbar\omega}{2} - \omega t\Big)\Big]\Big/\omega\sinh\Big(\frac{\beta\hbar\omega}{2}\Big)\Big\}\exp(-\Delta\epsilon\, t/\hbar) \quad . \tag{36}$$

$\theta''(t)$ is its second time derivative, and t^* denotes the location of the extremum of $\theta(t)$.

The function

$$\hat{C}(\omega) = \int_{-\infty}^{\infty} dt \langle \delta\mathcal{E}\, \delta\mathcal{E}(t)\rangle_A\, e^{i\omega t} \tag{37}$$

is the Fourier transform of the classical energy gap correlation function for the bath. Within a factor of frequency, $\hat{C}(\omega)$ is the spectral density of energy gap fluctuations. These relationships, provides a means to estimate quantal effects on electron transfer rates from a classical trajectory calculation.

Specifically, the spectral density can be determined from a computer simulation trajectory that is run in the reactant state. Figure 10 shows $\hat{C}(\omega)$ computed in this way for a simulation model of the ferrous-ferric pair in water and in heavy water. With this function determined, and with the thermodyanamic driving force, $\Delta\epsilon$, specified as well, $\theta(t)$ can be computed numerically from Eq. (36) for various values of t. In Marcus' normal region, an extremum in $\theta(t)$ will be found for t between 0 and $\beta\hbar$. In the inverted region, the extremum will be found at larger values. With the function $\nu(t)$ determined and the extremum identified, evaluation of the rate from Eq.(35) is immediate.

The spectral density, or $\hat{C}(\omega)$, decays to zero for large ω. Let ω_c denote a "cut-off" frequency, beyond which $\hat{C}(\omega)$ is effectively zero. A classical bath is one for which $\beta\hbar\omega_c \ll 1$. In this regime, the integrand in Eq.(36) can be expanded, the resulting integral is a quadratic function of time, and the rate constant reduces to the classical result, Eqs.(29) and (31). Generally, however, the spectral density contains significant high frequency contributions, in which case there are significant quantal corrections to

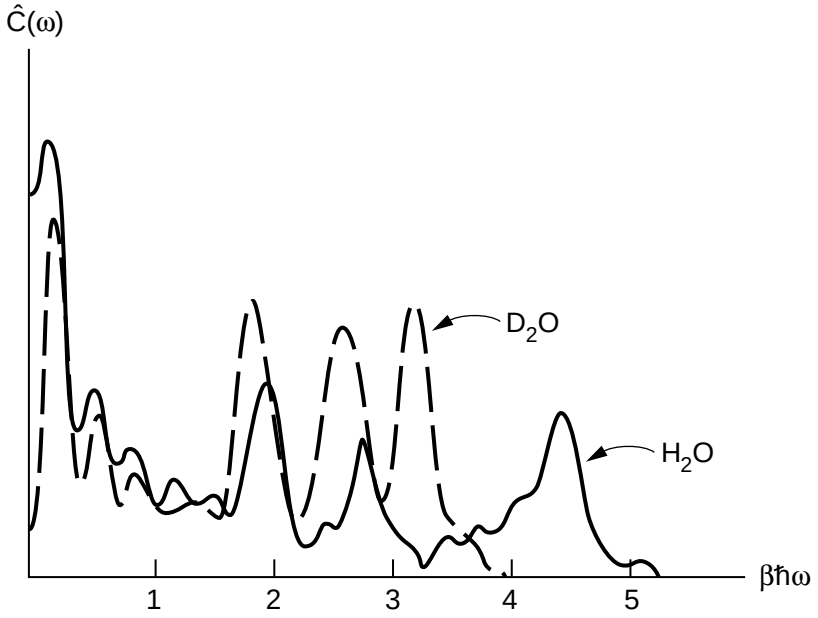

Fig. 10. – Fourier transform of the energy gap correlation function computed from classical computer simulation trajectories of the ferrous-ferric pair in water, and deuterated water.

the classical rate constant. The aqueous ferrous-ferric system provides an example, as is evident from the high frequency motions evident from the high frequency contributions to $\hat{C}(\omega)$ plotted in Fig.10 and the corresponding the short time decay of $C(t)$ plotted in Fig.8. Applying Eq.(35) with its spectral density as determined from simulation, see Fig.10, yield

$$k_{\rm ET}/k_{\rm ET}^{\rm classical} \approx 60, {\rm H_2O}, \approx 25, {\rm D_2O}. \tag{38}$$

Most pathways to electron transfer in normal and heavy water therefore involve significant aspects of nonclassical nuclear dynamics. Frequencies of librational motions in water are high, due to low proton (and deuterium) mass. These degrees of freedom can thus reach $\mathcal{E} = 0$ by tunneling into classically forbidden configurations. The quantal system thereby cuts the corners off the potential energy surface, Figs.6 or 7. Its free energy of activation is therefore effectively smaller than that of a classical system. In the inverted region, the distance between diabatic surfaces is smaller than in the normal region. (Consider, for example, the effect of dropping the right parabola in Fig.6, keeping the value of α fixed.) Thus, the effects of nuclear tunneling become further pronounced in the inverted region than found explicitly here for the normal region.

Imaginary time quantum path integral evaluation of the rate constants give results similar to Eq.(38). The path integral calculations are independent of the Gaussian approximation relating $k_{\rm ET}$ to the classical $C(t)$. The path integral calculations thus provide further support for the spin boson character used in the rate constant evaluation described above. Computer renderings of the imaginary quantum paths for water during the ferrous-ferric electron transfer show that the structures of these paths are similar to

those of classical trajectories during the first 20 to 30 fs following instantaneous charge transfer. In other words, the motions leading to the rapid relaxation depicted in Fig.8, mainly librations, are also the motions with which nuclei can tunnel through electron transfer transition state barriers.

The prediction from simulation, Eq.(38), provides an explanation of the observed isotope effect on the aqueous ferrous-ferric exchange,

$$k_{\rm ET}^{\rm H_2O}/k_{\rm ET}^{\rm D_2O} \approx 2. \tag{39}$$

There is less tunneling in heavy water than normal water because librations with heavy hydrogen occur at lower frequencies than those with normal hydrogen nuclei. Likely tunneling paths are shorter with heavy hydrogen than with normal hydrogen.

8. – Surface hopping model and exponential decay

Thus far in this Lecture, we have assumed that the rate constant for electron transfer is well defined, or equivalently, that relaxation from a non-equilibrium charge transfer state is exponential in time. From the previous lecture, we know that for this assumption to be valid, dynamics affecting the electron transfer must relax on time scales fast compared to $1/k_{\rm ET}$. Some modes of nuclear reorganization can persist for longer times thus invalidating the assumption. We can examine this issue with a classical surface hopping model of electron transfer.

Figure 11 depicts the fluctuations in the energy gap during a trajectory preceding electron transfer. In the surface hopping model, there is a non zero probability p for electron transfer only when the energy gap is zero, i.e., when $\mathcal{E}$ crosses $\mathcal{E}^* = -\Delta\epsilon/2$. For a given trajectory, the number of crossings in a time t is

$$N(t) = \int_0^t dt' \, |\dot{\mathcal{E}}(t')| \, \delta[\mathcal{E}(t') - \mathcal{E}^*] \tag{40}$$

Its average value is extensive in time. That is,

$$\nu = \langle N(t) \rangle_A \, / \, t = \langle |\dot{\mathcal{E}}| \rangle_A^* \, \langle \delta(\mathcal{E} - \mathcal{E}^*) \rangle_A \tag{41}$$

is the average frequency of crossing the electron transfer transition state.

If p is small enough, many crossings will occur before the electron will hop. In this case, or alternatively when visitation to the curve crossing point is rare, pertinent crossings can be treated as if they were uncorrelated. To the extent that subsequent recrossings are uncorrelated, the probability of N crossings occurring in a time t is given by the Poisson distribution,

$$\frac{1}{N!}(\nu t)^N e^{-\nu t}. \tag{42}$$

In this approximation, the probability that state A^-B will survive for a time t is therefore,

$$S(t) = \sum_N (1-p)^N \frac{1}{N!} \, (\nu t)^N \, e^{-\nu t} = e^{-kt}, \tag{43}$$

where

$$k = \nu p = (2\pi K^2/\hbar) \langle \delta(H_A - H_B) \rangle_A. \tag{44}$$

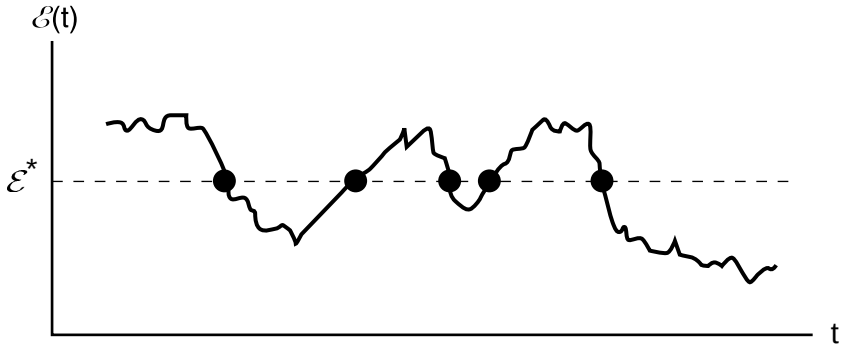

Fig. 11. – Energy gap fluctuations during a trajectory, depicting what is often refered to as "spectral diffusion". The dots indicate points where the net energy gap is zero.

The second equality of Eq.(44) is obtained by identifying the rate constant k with the classical golden rule rate constant, Eq.(28). This identification together with Eq.(41) leads to the Landau-Zener formula for p cited in Eq.(22).

Generally, however, the conditions leading to Poisson statistics and Eq.(43) may not hold, and the survival probability should be reduced no more than

$$S(t) = \langle (1-p)^{N(t)} \rangle_A \tag{45}$$

A cumulant expansion yields

$$S(t) = \exp[-\langle N(t) \rangle p] \exp\left\{ \frac{1}{2} [\langle (\delta N(t))^2 \rangle - \langle N(t) \rangle^2] p^2 \right\} \cdots . \tag{46}$$

For times larger than the bath relaxation times controlling $\mathcal{E}$, the fluctuation term tends to an extensive function of time. This fact follows from the same logic that leads one to expect, for the case of particle diffusion, that mean square displacements in particle position grow linearly in time for times larger than a momentum relaxation time. Thus, according to Eq.(46), $S(t)$ relaxes with the golden rule rate constant. As time proceeds, however, Eq.(46) shows that this relaxation rate eventually decreases. In particular, the long time decay occurs with a rate constant differing from the golden rule by an amount proportional to the typical variability in the rate of recrossings times the relaxation time for that variability. When either is very small, the entire relaxation is a simple exponential with the golden rule rate constant.

Equation (46) is useful for describing small deviations from exponential kinetics. For large deviations, other approximations are required for the evaluation of the average (45). In cases where either p or the frequency of recrossings fluctuates with large variability, but does so in ways that are slow compared to possible values of $1/k_{\mathrm{ET}}$, the deviation from exponential kinetics is described by the approximation of inhomogeneous kinetics,

$$S(t) = \int_0^\infty dk\, \rho(k)\, e^{-kt} \tag{47}$$

where $\rho(k)$ is the probability distribution function for a golden rule rate constant. Equation (47) is useful for interpreting electron transfer kinetics in proteins, where there are almost always collective motions contributing to the spectral density that are slower

than nearly any electron transfer process. Equation (47) is also justified when motions affecting the value of p are slow compared to the energy gap fluctuation relaxation times. This situation is often pertinent to the effect of variable inter-site distances (e.g., the separation of iron ions in the aqueous ferrous-ferric exchange).

9. – Summary

The basic idea in electron transfer theory is that redox states are localized electronic states, and that the coupling between different redox states is weak. As such, without photoinducement, electron transfer occurs only when two redox states are essentially degenerate. (If the coupling were strong, charge would distribute between the two states, and the concept charge transfer from one region of space to another would surely be inappropriate.) For this reason, the reaction coordinate for electron transfer is the energy gap between the reactant and product redox states. This gap fluctuates because the environment fluctuates. Thus, computational studies of electron transfer focus attention on the statistics of the energy gap, and from that statistics, rate constants can be calculated, employing golden rule formulas. To a remarkable extent, energy gap statistics is Gaussian, thus justifying the use of simple analytical formulas, such as Marcus' energy gap law in the classical case, and the golden rule rate constant formula involving the energy gap spectral density in the quantum case.

The role of nuclear dynamics is small, but still noteworthy in two regimes. First, fast components of the energy gap fluctuations (i.e., those with frequencies not small compared to $1/\beta\hbar$) can reach the region of interstate degeneracy and thus contribute to the electron transfer kinetics through nuclear tunneling pathways. Second, slow components (i.e., those with frequencies of motion that are not large compared to $1/k_{\mathrm{ET}}$) can lead to multiple exponential kinetics of electron transfer.

At normal chemical and biological conditions, fast motions that lead to nuclear tunneling are usually motions associated with protons. The high frequency librational motions of water molecules, for example, affect the dielectric response of liquid water, and thus their quantal nature are significant to aqueous electron transfer. What if these protons where also involved in chemistry — the breaking of chemical bonds — as can occur in the hydration of an acid? Here, an electron transfer reaction occurs with a concomitant proton transfer. What now is the reaction coordinate? This question presents a significant puzzle. In the next lecture we turn to the problem of determining transition pathways for classical systems. What should be done for analogous quantal cases remains unknown.

* * *

Peter Bolhuis, Gavin Crooks, Felix Csajka, Christoph Dellago, Phillip Geissler, Zoran Kurtovich, Ka Lum and Xueyu Song provided many helpful suggestion for this lecture write-up. In addition, Gavin Crooks and Phillip Geissler provided extensive and invaluable help in preparing the manuscript. My research on electron transfer processes has been supported by the US Department of Energy.

REFERENCES

In his Nobel Prize lecture, Rudolph Marcus described the history and many implications of his theory of electron transfer. This lecture is published in R.A.Marcus, *Rev. Mod. Phys.* **65**, 599 (1993).

A commonly cited review on the subject of electron transfer is R.A.Marcus and N.Sutin, *Biochim. Biophys. Acta* **811**, 265 (1985). More mathematical detail, and some discussion of the spin boson model is found in my Les Houches lectures: D. Chandler in *Les Houches 51*, Part 1, ed. by D. Levesque, J.-P. Hansen and J. Zinn-Justin (North Holland, Amsterdam, 1991),p.193. For example, a compact quantum path integral derivation of Eq.(35) is given in those lectures. A more traditional derivation of Eq.(35) is given in R.P.Van Duyne and S.F.Fischer, *Chem. Phys.* **5**,183(1974). Detailed analysis of the spin boson model in many regimes, including electron transfer, is the subject of the book by U. Weiss, *Quantum Dissipative Systems* (World Scientific, Singapore, 1993).

Studies of solvation dynamics, like that illustrated in Fig.8., have been pioneered by Graham Fleming and Mark Maroncelli, and reviewed in M.Maroncelli, *J. Mol. Liquids* **57**, 1 (1993)

To the extent that dynamical response to charge transfer is not linear, one must be concerned with the accuracy of Eq.(35). Without recourse to the Gaussian approximation, however, it is still possible to numerically evaluate $k_{\rm ET}$ from Eq.(26). The evaluation is carried out numerically, employing imaginary time quantum path integrals, as suggested in P.G.Wolynes, *J. Chem. Phys.* **87**, 6559 (1987). Calculations of this type concerning electron and nuclear tunneling in the aqueous ferrous-ferric exchange are described in J.S.Bader, R.A.Kuharski and D.Chandler, *J. Chem. Phys.* **93**, 230 (1990); and in M.Marchi and D.Chandler, *J. Chem. Phys.***95**, 889 (1991).

Slow energy gap fluctuations and resulting complex electron transfer kinetics in photosynthetic reaction centers, is discussed in J.N.Gehlen, M.Marchi and D.Chandler, *Science* **263**, 499 (1994).